Available online at www.sciencedirect.com
SCIENCE DIRECT®
Journal of Solid State Chemistry 177 (2004) 415–424
JOURNAL OF SOLID STATE CHEMISTRY
http://elsevier.com/locate/jssc

Solid state phase equilibria in the Gd–Si–B system at 1270 K

V. Babizhetskyy,[1] J. Roger, S. Députier, R. Jardin, J. Bauer, and R. Guérin*

Laboratoire de Chimie du Solide et Inorganique Moléculaire, UMR CNRS 6511, Université de Rennes 1, Institut de Chimie, Campus de Beaulieu, Avenue du Général Leclerc, F-35042 Rennes Cedex, France

Received 25 September 2002; accepted 6 February 2003

Abstract

Solid state phase equilibria in the ternary Gd–Si–B phase diagram have been proposed at 1270 K using X-ray diffraction, scanning electron microscopy and electron probe microanalysis. Prior to this work, the binary systems Gd–B, Gd–Si and Si–B have also been reinvestigated. The main characteristic of the ternary diagram is the occurrence of two new ternary compounds $Gd_5Si_2B_8$ and $Gd_5Si_3B_{0.64}$. The former crystallizes in tetragonal symmetry, space group $P4/mbm$ with unit cell parameters $a = 7.2665(3)$, $c = 8.2229(7)$ Å, the second one presents hexagonal symmetry, space group $P6_3/mcm$ with unit cell parameters $a = 8.5080(4)$, $c = 6.4141(2)$ Å. The X-ray structures of the two structurally related phases $Gd_5Si_3B_{0.64}$ and host binary Gd_5Si_3 have been refined from three-dimensional single-crystal intensity data to the final R values of 0.036 ($R_w = 0.046$) and 0.046 ($R_w = 0.055$) for 457 and 401 reflections, respectively with $[F > 4\sigma(F)]$. Both structures exhibit the Mn_5Si_3-type structure, with in addition for $Gd_5Si_3B_{0.64}$ a partial occupancy by boron of the normally vacant interstitial site at the center of the Gd_6 octahedron, which corresponds to the origin of the unit cell. Bonding between the interstitial boron atoms and the gadolinium ones forming the Gd_6B polyhedra is indicated by the decrease in the corresponding Gd–Gd distances and consequently in the unit cell volume. Finally, the Gd–Si–B phase diagram is compared with the previously reported Er–Si–B, at 1070 K.

Keywords: Ternary rare earth borosilicides; Phase diagram; X-ray diffraction; Electron microscopy; Crystal structure

1. Introduction

Many studies have been devoted to the crystal chemistry and physical properties of ternary compounds comprising a rare earth, boron and carbon [1–5]. In addition, theoretical calculations have been performed in order to rationalize the nature of the chemical bond within the boron–carbon sublattice [6–9]. The same approach has been adopted for research on the ternary rare earth borosilicides. Up to now, literature is very poor concerning this topic. Ternary R–Si–B phase diagrams for R= La, Ce, Er and Y have been constructed from bulk materials after arc melting and annealing of the samples at 1070 K [10,11], but the occurrence of ternary phases has not been mentioned. Small solubility of boron in the R_5Si_3 silicides (R= Gd, Tb, Dy) has been detected but the limits of solid solutions have not been established [12]. The first ternary rare earth borosilicides have been synthesized but with very high boron contents, like $YSiB_{44}$ [13], $YSi_{4.6}B_{17.6}$ [14], $TbSi_{1.2}B_{41}$ [15] and $Y_{1-x}Si_3B_{12}$ ($0.2 < x < 0.4$) [16], showing icosahedral boron units. The only reported gadolinium borosilicide $GdSi_{1.2}B_{41}$ belongs to this boron-rich family [17]. Similar phases stabilized by carbon in addition have also been discovered recently, like for example $ScC_{0.65}Si_{0.07}B_{12}$ [16], $Sc_{0.8}C_{0.53}Si_{0.06}B_{9.6}$ [18] and $Tb_{3-x}C_2Si_8B_{36}$ [19].

The occurrence of ternary rare earth borosilicides could be technologically important. Indeed, rare earth silicides have been currently extensively studied because of their applications in semiconductor technology [20,21]. Especially, these binaries are of great interest since they can be formed epitaxially on monocrystalline silicon [22]. Moreover, they are characterized by the lowest Schottky barrier heights (SBH) on n-type Si (0.3 eV for $ErSi_{2-x}$), with potential applications in infrared detectors [23].

The present paper deals with the experimental determination of the solid state phase equilibria in the

*Corresponding author. Fax: +02-99-63-57-04.
E-mail address: roland.guerin@univ-rennesl.fr (R. Guérin).
[1] Present address: Max-Planck-Institute, Heisenbergstrasse 1, Postfach 800665, D-70569 Stuttgart, Germany.

0022-4596/$ - see front matter © 2003 Elsevier Inc. All rights reserved.
doi:10.1016/j.jssc.2003.02.011

Gd–Si–B system at 1270 K. The choice of gadolinium results from its position at the interface of light and heavy rare earths. Prior to the ternary diagram, it has been proceeded to a re-examination of the binary phases belonging to the Gd–Si, Gd–B and Si–B systems, previously reported in literature. The ternary phase diagram reveals two new gadolinium borosilicides $Gd_5Si_2B_8$ and $Gd_5Si_3B_{0.64}$. The crystal structure of the latter compound will be discussed herein together with the one of Gd_5Si_3, which we have determined for comparison. Finally, the isothermal section of the Gd–Si–B phase diagram will be compared with the previously reported Er–Si–B at 1070 K.

2. Experimental

2.1. Sample preparation

Polycrystalline samples in the ternary phase diagram were prepared from pure elements: gadolinium as ingots (purity higher than 99.9%), silicon (>99.99%) and boron (>99%) as powders, all supplied by Strem Chemicals.

Suitable amounts of powder and freshly filed chips of the constituents were mixed together and pressed into pellets. The melting of the samples (about 800 mg each) was performed with the help of an arc furnace using a non-consumable thoriated tungsten electrode under Ti/Zr-gettered argon atmosphere. To ensure homogeneity, the samples were turned over and re-melted several times. Finally, to reach thermodynamic equilibrium, the so-obtained samples were sealed in evacuated silica tubes, heat treated at 1270 K for 1 month and subsequently quenched in cold water.

2.2. Powder diffraction and microprobe analysis

The samples were cut into several pieces. One part of each sample was pulverized and analyzed by X-ray diffraction (XRD) using a powder diffractometer (CPS 120 INEL) equipped with a position-sensitive detector ranging 120° in 2θ. Elemental germanium (99.9999%, $a_{Ge} = 5.657905$ Å) served as an internal standard. The unit cell parameters were refined with the help of the CSD package program [24]. A second part was kept for research of single crystals in the molten matrix. The last part was embedded in epoxy resin and polished down to 0.25 mm diamond grade. The sample was then coated with either a gold or graphite thin layer to obtain a good surface conductivity. Backscattered electron imaging was done with a Jeol JSM-6301F scanning electron microscope (SEM). Quantitative composition analyses (EPMA) were performed either on a Jeol JSM-6400 by energy-dispersive spectroscopy (EDS) of X-rays or on a Camebax SX 50 using wavelength-dispersive spectroscopy (WDS) of X-rays (GdB_2C_2, GdB_4, GdSi and/or elemental Si as standards). EPMA measurements were found to be in good agreement with phase compositions observed by powder diffraction and empirical formulas deduced from single-crystals data refinement, moreover no contamination by oxygen and/or carbon was detected.

2.3. Single-crystal X-ray diffraction

Single-crystal intensity data were collected at ambient temperature applying a Nonius Kappa CCD X-ray area-detector diffractometer using Mo$K\alpha$ radiation ($\lambda = 0.71073$ Å).

Data collection strategy was performed with the help of the program COLLECT [25] and reflections were corrected using the program DENZO of the Kappa CCD software package [26]. Owing to the size of the single crystals, no precise absorption correction was done. Structures were solved by direct methods (SIR 97 [27]) and least-squares refinements, difference Fourier syntheses were run with the CSD program package [24]. The program DIAMOND [28] was used to prepare the drawings of the structural units.

3. Results and discussion

3.1. Constituent binaries

Prior to discussing the experimental data obtained in the present study for the Gd–Si–B ternary system at 1270 K, a perfect knowledge of the binary phases which border the diagram has been necessary.

3.1.1. Gd–B system

Five intermediate phases in the Gd–B system are mentioned in literature: GdB_2, Gd_2B_5, GdB_4, GdB_6 and GdB_{66} [29,30]. To check these results, numerous samples in the Gd–B system have been prepared using the synthetic conditions of the ternary samples. The combination of XRD together with EPMA experiments leads to the presence of the three binaries Gd_2B_5, GdB_4, GdB_6 at the reaction temperature. If GdB_2 has been observed after arc melting, it disappears completely after annealing, confirming the binary Gd–B system. The boron-rich corner including GdB_{66}, with icosahedral boron units, has been less investigated owing to the sluggish peritectic reaction between the liquid and GdB_6 [29]. As an example, a backscattered electron image of a sample with composition Gd/B = 10/90 shows only GdB_6 and elemental boron (Fig. 1a). The very thin peritectic layers of GdB_{66} which should be around the grains of GdB_6 cannot be observed. The structural data for all the binaries in the Gd–B system are summarized in Table 1.

3.1.2. Gd–Si system

In the same manner, the binaries belonging to the Gd–Si system have been studied. Five gadolinium silicides are mentioned in Refs. [29,30]. Three out of the binaries correspond to stoichiometric compounds i.e., Gd_5Si_3, Gd_5Si_4 and GdSi, while the other two silicides $GdSi_2$ and $GdSi_{2-x}$ exhibit a narrow range of homogeneity. Moreover, the last two are mentioned to present polymorphic modifications: α-$GdSi_2$ (orth., *Imma*) for $T<673$ K and β-$GdSi_2$ (tetrag., $I4_1/amd$) for $T>673$ K, α-$GdSi_{2-x}$ (hex., $P6/mmm$) for $T<1300$ K and β-$GdSi_{2-x}$ (no reported structural data) for $T>1300$ K. The study of the Gd–Si binary system at 1270 K confirmed unambiguously the occurrence of the binaries Gd_5Si_3 (Mn_5Si_3 type), Gd_5Si_4 (Sm_5Ge_4 type) and GdSi (FeB type). For the other binaries $GdSi_2$ and $GdSi_{2-x}$, only the α-form (orthorhombic and hexagonal, respectively) has been observed on XRD patterns. As annealings have been made at 1270 K, the very low transition temperature (673 K) given in literature for the binary $GdSi_2$ seems questionable. Moreover, the β-$GdSi_2$ form has not been observed even after arc melting. The structural data for the binary silicides are reported in Table 1.

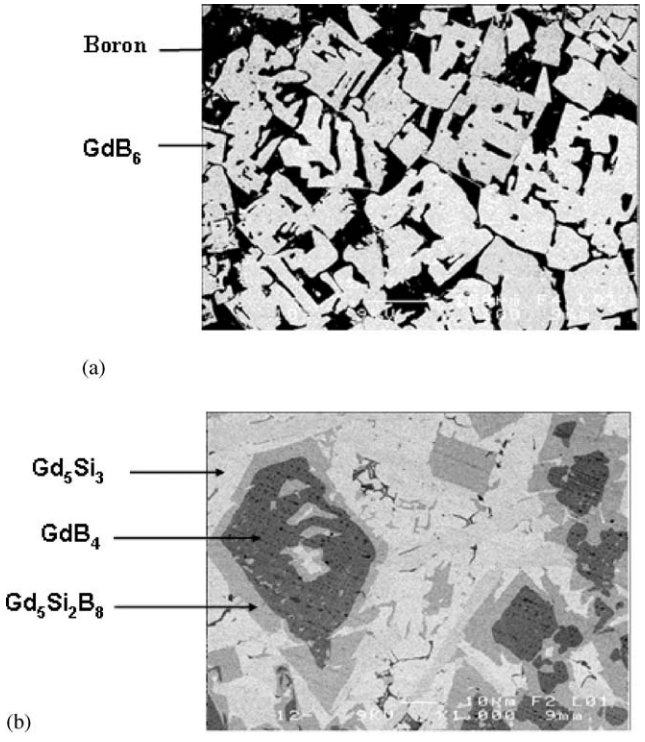

Fig. 1. Backscattered electron images: (a) sample with composition Gd/B = 10/90. Elemental boron (black) and binary GdB_6 (gray or white) are only present. Differences between gray and white grains are due to orientation effect. No trace of peritectic layers of GdB_{66} could be observed. (b) Formation of $Gd_5Si_2B_8$ (dark gray) from peritectic reaction between GdB_4 (black) and Gd_5Si_3 (white). For some crystals of $Gd_5Si_2B_8$, transformation is completely achieved while for the others, it is going on. The very small difference between the nearly white grains observed is due probably to the occurrence of traces of inserted boron in Gd_5Si_3.

3.1.3. Si–B system

Previous investigations have revealed that at least three phases occur in the binary Si–B system. [29–33]. The first one is a solid solution with composition range close to SiB_3, the second one is a stoichiometric compound SiB_6 and the last one corresponds to an extended solid solution with formula SiB_n (between 93.23 and 97 at% B). The solubility of silicon in boron is about 3 at% at 2250 K while 3–4 at% of boron are dissolved in silicon at 1650 K [29]. In addition, the crystal structure of a rhombohedral boron-rich silicide Si_8B_{305} (97.4 at% B) has also been proposed [34,35].

Combining XRD and EPMA, a silicon-rich phase with approximate formula $Si_{99}B$ having cubic symmetry

Table 1
Gd–Si–B constituent binary phases, crystal structures and lattices parameters

Phase	Type structure, Pearson symbol	Space group	Lattice parameters (Å)			
			a	*b*	*c*	*β*
GdB_2	AlB_2, hP3	$P6/mmm$	3.319(2)		3.944(3)	
Gd_2B_5	Gd_2B_5, mP28	$P2_1/c$	7.205(9)	7.202(7)	7.283(8)	102.93(7)
GdB_4	ThB_4, tP20	$P4/mbm$	7.148(3)		4.050(2)	
GdB_6	CaB_6, cP7	Pm-$3m$	4.1148(4)			
[a]GdB_{66}	ThB_{66}, cF1880	Fm-$3c$	23.474(3)			
[b]Gd_5Si_3	Mn_5Si_3, hP16	$P6_3/mcm$	8.5133(2)		6.4206(3)	
Gd_5Si_4	Sm_5Ge_4, oP36	$Pnma$	7.548(4)	14.869(9)	7.841(5)	
GdSi	FeB, oP8	$Pnma$	7.971(4)	3.856(2)	5.738(4)	
α-$GdSi_2$	$GdSi_2$, oI12	$Imma$	4.120(3)	4.043(3)	13.549(9)	
[a]β-$GdSi_2$	$ThSi_2$, tI12	$I4_1/amd$	4.0438(6)		13.802(5)	
α-$GdSi_{2-x}$	AlB_2, hP3	$P6/mmm$	3.894(2)		4.194(3)	
[a]SiB_3	B_6P, hR14	R-$3m$	6.319(5)		12.713(10)	
[a]SiB_6	SiB_6, oP280	$Pnnm$	14.397(7)	18.318(9)	9.911(7)	
[a]SiB_n	Deriv. β boron	R-$3m$	11.09(5)		23.85(5)	

[a] Lattice constants from Ref. [30].
[b] Lattice constants on single crystal counter data.

has been evidenced, which belongs to the miscibility domain of boron in silicon. The unit cell parameter $a = 5.439(1)$ and $5.424(2)$ Å for Si and $Si_{99}B$, respectively, agrees well with the covalent radius decrease (1.17 Å for Si instead of 0.87 Å for B) [36]. Another phase having rhombohedral symmetry (space group *R*-3*m*) has also been obtained, but the actual composition $Si_{15}B_{290}$ (95.1 at% B), within the SiB_n solid solution, is somewhat different from the previous reported Si_8B_{305}. The hexagonal unit cell parameters of the phase $Si_{15}B_{290}$ correspond to $a = 11.0152(3)$ and $c = 23.8625(8)$ Å. EPMA together with XRD experiments lead to consider $Si_{15}B_{290}$ and Si_8B_{305} as two different phases. Single crystal structure determination is at the present time in progress [37]. Finally, a last phase has been evidenced by XRD and EPMA but in mixtures of several phases. Unfortunately, no single crystals of good quality have been obtained at present. The chemical formula deducted from EPMA concludes to the formula "SiB_4".

It is clear that our results at 1270 K in the Si–B system are not completely consistent with the crystallographic data given in literature, especially for binary SiB_6 (Table 1). Indeed, annealings at 1270 K should be much longer to complete the decomposition of metastable SiB_3 in SiB_6 and silicon [29,38]. The inconsistencies in the Si–B system must be attributed for a large part to the different synthesis procedures and especially to the reaction temperature, the cooling rate as well as the quality of starting elements (purity and powder size). A more detailed study of the Si–B system will be done again for more clarity.

3.2. Ternary Gd–Si–B phase diagram

The experimental Gd–Si–B ternary diagram at 1270 K is proposed in Fig. 2a. Under our experimental conditions, the binaries that border the diagram at the reaction temperature are: Gd_2B_5, GdB_4, GdB_6, Gd_5Si_3, Gd_5Si_4, GdSi, α-$GdSi_2$ and α-$GdSi_{2-x}$ (*vide supra*). For the Si–B system, at the present time, the four phases Si_8B_{305}, $Si_{15}B_{290}$, SiB_6 and "SiB_4" have been considered.

The solid state phase equilibria of the Gd–Si–B system have been deduced from a total of about 50 samples which have been first studied by X-ray diffraction. EPMA experiments by EDS on most of the samples and by WDS on selected samples have confirmed in a second time the occurrence of mono-, di- or triphasic regions (Table 2).

The main feature of this isothermal section is the discovery of the two ternary gadolinium borosilicides $Gd_5Si_2B_8$ (Gd/Si/B = 33.3/13.3/53.3 at%) and $Gd_5Si_3B_{0.64}$ (57.9/34.7/7.4 at%). The description of their structure determined on single crystals has been done [39]. The symmetry has been found to be tetragonal [space group *P*4/*mbm*) and hexagonal (space group $P6_3/mcm$) for $Gd_5Si_2B_8$ and $Gd_5Si_3B_{0.64}$, respectively (*vide infra*).

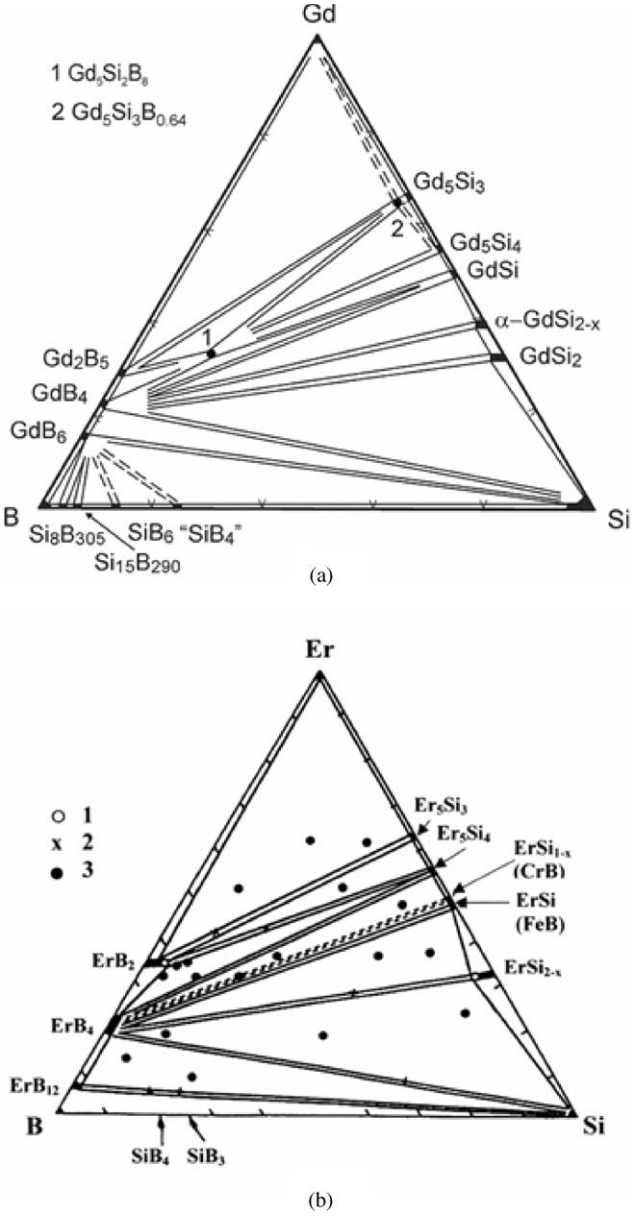

Fig. 2. Solid state phase equilibria in the ternary systems: (a) Gd–Si–B at 1270 K from present work, (b) Er–Si–B at 1070 K from Ref. [11]. Axes are in at%. Setting of sample compositions has been omitted in (a) for more clarity.

Under our experimental conditions, no trace of the ternary $GdSi_{1.2}B_{41}$, previously reported [17] has been found.

The second characteristic of the diagram results from number of tie lines which connect most of the Gd–B and Gd–Si binaries. For example, the boride GdB_4 is in thermodynamic equilibrium with α-$GdSi_2$, α-$GdSi_{2-x}$ and GdSi, but also with the ternary compound $Gd_5Si_2B_8$ and elemental silicon. $Gd_5Si_2B_8$ itself is in equilibrium with most of the binaries, except the silicides α-$GdSi_2$, α-$GdSi_{2-x}$ and GdB_6. To illustrate these results, some significant examples are proposed. First, XRD patterns

Table 2
Gross sample compositions and phases identified by X-ray diffraction and EPMA for 1270 K isotherm

Sample gross composition (at%)			Phases identified by X-ray diffraction	Composition of phases by EPMA (at%)[b]		
Gd	Si	B		Gd	Si	B
55	10	35	Gd_5Si_3[a]	62.7	37.3	—
			Gd_2B_5	28.9	—	71.1
			Gd	99.9	—	—
42.5	16.5	41	Gd_5Si_3	61.5	38.5	—
			Gd_2B_5	27.9	—	72.1
			$Gd_5Si_2B_8$	31.6	12.1	56.3
40	20	40	GdSi	49.5	50.5	—
			GdB_4 (trace)	20.5	—	79.5
			$Gd_5Si_2B_8$	31.7	12.0	56.3
33	17	50	Gd_5Si_3	62.8	37.2	—
			GdB_4	19.8	—	80.2
			$Gd_5Si_2B_8$	31.8	12.4	55.8
33	33	33	α-$GdSi_{2-x}$	37.7	62.3	—
			GdSi	49.5	50.5	—
			GdB_4	19.5	—	80.5
33	53	13	α-$GdSi_{2-x}$	39.7	60.3	—
			α-$GdSi_2$	34.1	65.9	—
			GdB_4	18.7	—	81.3
20	55	25	α-$GdSi_{2-x}$	34.1	65.9	—
			GdB_4	19.5	—	80.5
			Si	—	99.9	—
10	25	65	GdB_6	14.8	—	85.2
			Si	—	99.9	—
0	10	90	SiB_n	—	4.8	95.2
			Si	—	99.9	—
0	5	95	SiB_n	—	4.2	95.8
			Si	—	99.9	—

[a] In fact either Gd_5Si_3 or $Gd_5Si_3B_{0.64}$.
[b] Estimated standard deviations less than 2 at%.

(not presented here) of a sample with nominal composition Gd/Si/B = 33/53/13 shows a mixture of the three binaries GdB_4, α-$GdSi_2$ and α-$GdSi_{2-x}$. In a first time, insufficient contrasting effect on backscattered electron images did not allow to identify grains of each silicide. The use of optical microscopy with polarization light confirmed effectively the presence of the three phases. However, at the present time, it is difficult to conclude on the exact nature of binary silicides. It seems probable that one phase at least, otherwise both phases contain small amounts of boron.

The second example concerns the formation of the ternary $Gd_5Si_2B_8$. Indeed, this phase has never been obtained as a pure phase, but in mixtures of phases containing Gd_5Si_3 and/or GdB_4. The concentration profiles by EPMA on two samples with nominal compositions Gd/Si/B = 40/20/40 and 28/5/67 are given in Fig. 3, while the backscattered electron image in Fig. 1b shows the formation reaction of the ternary borosilicide $Gd_5Si_2B_8$. It is clear that the formation of $Gd_5Si_2B_8$ results from a peritectic reaction between both binaries GdB_4 and Gd_5Si_3. Therefore, when the sample is silicon-rich (Fig. 3a), an excess of Gd_5Si_3 together with $Gd_5Si_2B_8$ is found after peritectic reaction. The inverse scheme is observed when the sample is boron-rich with the presence of an excess of GdB_4 together with $Gd_5Si_2B_8$ (Fig. 3b).

The solid state phase equilibria of the Gd–Si–B system at 1270 K resembles to the *R*–Si–B ones at 1070 K (*R*= La, Ce, Er and Y), previously reported [10,11]. Although no ternary phase has been mentioned for the last ones, the general aspect remains the same, especially from a tie lines point of view. For example, the preponderant part of the rare earth tetraboride RB_4 is evident, since it is in thermodynamic equilibrium with most of the binary silicides (Fig. 2b). It should be noted that the occurrence of a narrow miscibility domain of boron in binary $ErSi_{2-x}$ which agrees well with our own results, not yet published [40], justifies a more attention in this area for the Gd–Si–B system.

3.3. Crystal structures

The crystal structures of $Gd_5Si_2B_8$ and $Gd_5Si_3B_{0.64}$ have been solved on single crystals [39]. The structure of $Gd_5Si_2B_8$ is of a new type and exhibits a tetragonal

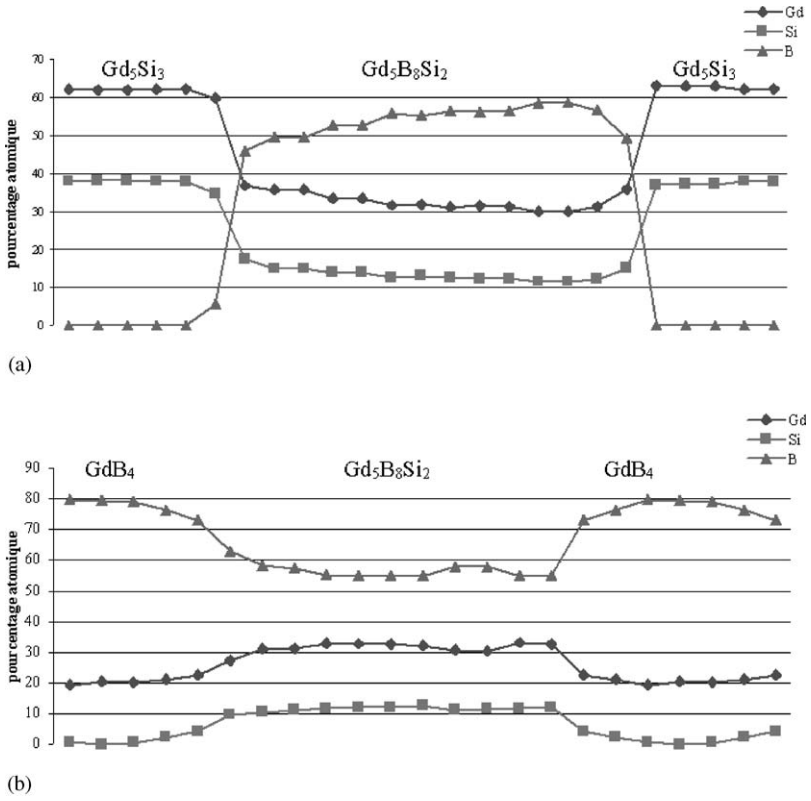

Fig. 3. Concentration profiles of samples with compositions (a) $Gd_{40}Si_{20}B_{40}$, (b) $Gd_{28}Si_5B_{67}$.

symmetry, space group $P4/mbm$ with the unit cell parameters $a = 7.2665(3)$, $c = 8.2229(7)$ Å and $Z = 2$. It can be viewed as resulting from the intergrowth of both structure types GdB_4 (or ThB_4) and U_3Si_2 [41,42]. The two structural layers, the first containing Gd and B atoms as in GdB_4, the second one with Gd and Si atoms as in U_3Si_2 (Gd instead of U atoms), are placed alternatively along the [001] direction. The boron and silicon subnets are independent of each other in such a way that no boron–silicon bond occurs in the structure, contrary to the numerous and strong Si–Si and B–B covalent bonds. A more detailed description of the structural type $Gd_5Si_2B_8$ (and isostructural $R_5Si_2B_8$ compounds with R = Sm and Tb) together with theoretical calculations is proposed elsewhere [43].

The ternary phase $Gd_5Si_3B_{0.64}$ has been obtained from boron-poor samples. In the absence of additional experimental data, it is difficult to conclude about the nature of this ternary, since XRD patterns of $Gd_5Si_3B_{0.64}$ and Gd_5Si_3 are nearly identical. Are we in the presence of an interstitial phase on the boron-rich limit of the solid solution $Gd_5Si_3B_x$, as previously suggested [12] or is $Gd_5Si_3B_{0.64}$ a proper phase? In the absence of complementary data, we cannot decide at the moment.

Single crystals of $Gd_5Si_3B_{0.64}$ could be extracted from molten samples and were suitable for structure determination. EPMA experiments detected the presence of boron within the crystals but no accurate determination of boron content could be done by this way. To compare structural results between the ternary $Gd_5Si_3B_{0.64}$ and the host binary Gd_5Si_3, it has been also proceeded to the single crystal structure determination of Gd_5Si_3. The crystallographic data and details of data collection are summarized in Table 3. The unit cell parameters and volume decrease from the binary to the ternary can be attributed to additional Gd–B interactions in the ternary (*vide infra*).

Both structures have been solved by direct methods and least-squares refinements. The gadolinium and silicon atoms have been placed easily and the successive steps were run by introducing isotropic then anisotropic displacement parameters. In order to locate the boron atoms in the ternary, difference Fourier maps have been established and revealed a residual electronic density peak at the origin of the hexagonal unit cell (Fig. 4a). The attribution of this peak to boron led to the final reliability factors given in Table 3. Final difference Fourier synthesis did not mention any significant electronic density peaks (Fig. 4b and c). Atomic positional and displacement parameters are listed in Table 4 and selected interatomic distances are given in Table 5. Observed and calculated structure factors can be obtained from the authors on request.

Table 3
Crystal data, intensity collection and refinement for Gd_5Si_3 and $Gd_5Si_3B_{0.64}$

Empirical formula	Gd_5Si_3	$Gd_5Si_3B_{0.64}$
Formula weight ($g\,mol^{-1}$)	870.51	877.43
Crystal system	Hexagonal	Hexagonal
Space group	$P6_3/mcm$	$P6_3/mcm$
a (Å)	8.5133(2)	8.5080(4)
c (Å)	6.4206(3)	6.4141(2)
V (Å^3)	403.00(4)	402.09(5)
Z, calculated density ($g\,cm^{-3}$)	2; 7.173(1)	2; 7.247(1)
Crystal shape	Platelet	Platelet
Crystal size (mm^3)	$0.14 \times 0.08 \times 0.04$	$0.08 \times 0.06 \times 0.055$
Linear absorption coefficient (mm^{-1})	42.17	42.27
Refinement limits		
θ (deg)	3–37	1–35
h, k, l	$-14<h<11$;	$-13<h<13$;
	$-9<k<14$;	$-13<k<13$;
	$-10<l<10$	$-10<l<10$
Reflections collected	8764	7324
Independent reflections (R_{int})	1370 (0.058)	1189 (0.061)
Reflections in refinement ($F>4\sigma(F)$)	401	457
Variable parameters	12	14
Refinement	F	F
$R(F)$	0.046	0.036
R_w with $w=1/[\sigma(F_o^2)+(pF_o^2)$	0.055 ($P=0.0009$)	0.043 ($P=0.0009$)
Extinction coefficient (Sheldrick-1)	$1.05(8)\times10^{-3}$	$5.2(4)\times10^{-4}$
Scale factor	1.115(4)	1.590(4)
Goodness-of-fit	1.01	1.00

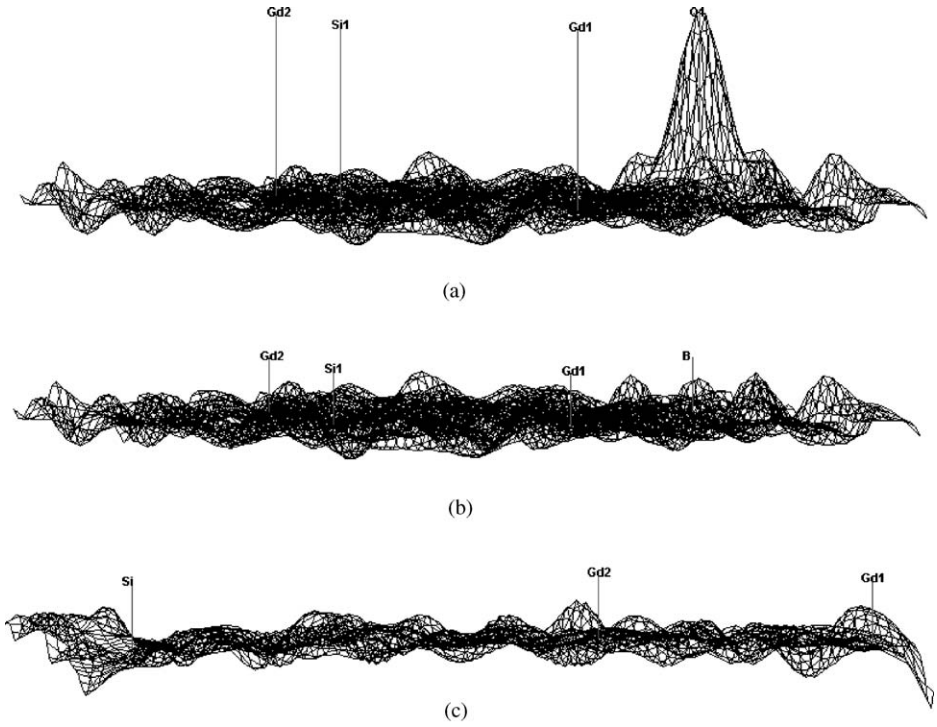

Fig. 4. Difference Fourier maps for $Gd_5Si_3B_{0.64}$ (a) before and (b) after introducing boron in refinement, (c) for Gd_5Si_3.

The structure of $Gd_5Si_3B_{0.64}$ is similar to the one of Gd_5Si_3 of Mn_5Si_3 type [44]. Most of rare earth silicides, having same atomic composition, are known to belong to the family of Mn_5Si_3-type structures [30]. Fig. 5a shows a projection of the structure on the (001) plane. The Gd1 atoms located at (1/3, 2/3, z) where $z=0$ and 0.5 are coordinated by six silicon atoms in a coordination scheme of irregular trigonal antiprisms. The Gd2

Table 4
Atomic positional and isotropic displacement parameters for Gd_5Si_3 and $Gd_5Si_3B_{0.64}$

	Atom	Position	x	y	z	B_{eq}.(Å^2)[a]
	Gd1	4*d*	1/3	2/3	0	0.94(2)
Gd_5Si_3	Gd2	6*g*	0.24240(8)	0	1/4	0.83(2)
	Si	6*g*	0.6044(4)	0	1/4	0.84(11)
	Gd1	4*d*	1/3	2/3	0	1.08(2)
$Gd_5Si_3B_{0.64}$	Gd2	6*g*	0.24103(7)	0	1/4	0.98(2)
	Si	6*g*	0.6035(4)	0	1/4	0.97(10)
	B[b]	2*b*	0	0	0	1.0(8)

[a] $B_{eq} = 1/3[B_{11}a^{*2}a^2 + \cdots 2B_{23}b^*c^*bc\cos(\alpha)]$.
[b] Occupancy factor: $\tau = 0.64(8)$.

Table 5
Main interatomic distances (Å) of Gd_5Si_3 and $Gd_5Si_3B_{0.64}$ and their ESDs

Gd_5Si_3		$Gd_5Si_3B_{0.64}$	
Gd1–6Si	3.0669(2)	Gd1–6Si	3.0625(3)
Gd1–2Gd1	3.2104(3)	Gd1–2Gd1	3.2071(2)
Gd1–6Gd2	3.6641(2)	Gd1–6Gd2	3.6686(3)
Gd2–2Si	2.9413(2)	Gd2–2B	2.6031(6)
Gd2–1Si	3.0818(7)	Gd2–2Si	2.9439(4)
Gd2–2Si	3.4651(4)	Gd2–1Si	3.0841(8)
Gd2–2Gd2	3.5743(6)	Gd2–2Si	3.4691(3)
Gd2–4Gd1	3.6641(4)	Gd2–2Gd2	3.5518(7)
Gd2–4Gd2	3.8163(3)	Gd2–4Gd1	3.6686(5)
		Gd2–4Gd2	3.8066(3)
Si–2Gd2	2.941(3)		
Si–4Gd1	3.067(1)	Si–2Gd2	2.944(3)
Si–1Gd2	3.082(3)	Si–4Gd1	3.063(1)
Si–2Gd2	3.465(1)	Si–1Gd2	3.084(3)
		Si–2Gd2	3.469(1)
		B–6Gd2	2.6031(6)

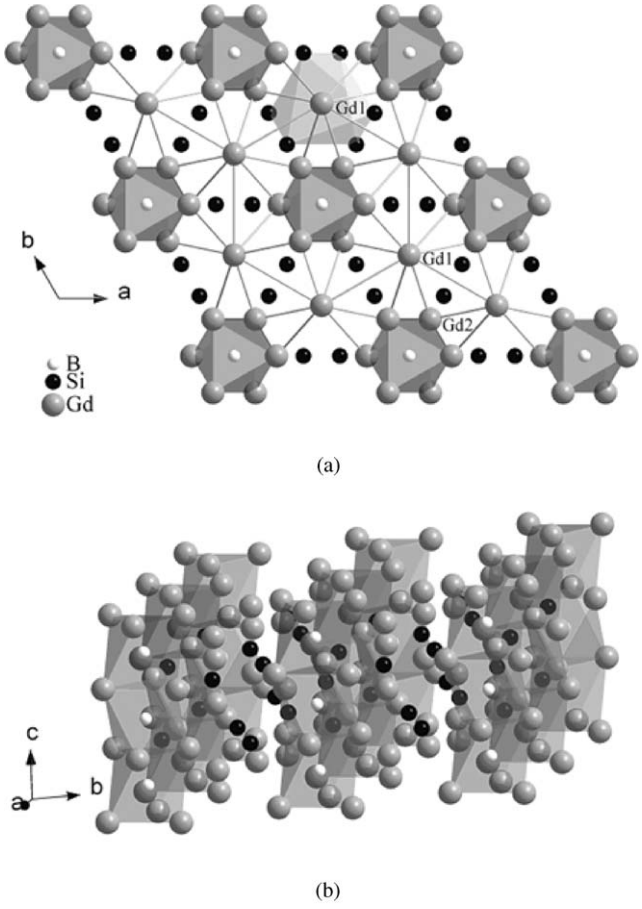

Fig. 5. Crystal structure of $Gd_5Si_3B_{0.64}$: (a) in projection on the (001) plane, (b) along the [001] direction. The Gd_6 octahedra containing boron atoms are emphasized.

atoms located around the origin of the unit cell form octahedra which develop infinitely by common faces along the [001] direction (Fig. 5b).

Within the cavity of each octahedron is an interstitial site at (0,0,0) and (0,0,0.5) which is normally vacant in the binary Gd_5Si_3. With two formula units per cell, up to two interstitial boron atoms could be accommodated per unit cell. This yields a formula for the fully doped structure corresponding to $Gd_5Si_3B_{1.0}$. In fact, from structure refinement, the site is only 64% occupied, leading to the final formula $Gd_5Si_3B_{0.64}$. This structural result can be compared with the one of $Ti_5Si_3B_{0.45}$, recently reported in Ref. [45]. These two ternaries belong to the Nowotny phases [46]. The metallic radius of gadolinium (1.79 Å) larger than the one of titanium (1.47 Å) may explain the higher boron content in the gadolinium-containing structure [47].

Addition of boron in the interstitial sites within the chains of Gd_6 octahedra involves Gd2–B bonds, as suggested by the cavity contraction, although the Gd2 atoms are now surrounded by seven metalloïd atoms (5 Si + 2 B), instead of five silicon atoms in Gd_5Si_3. The overall coordination number (CN) of Gd2 atoms is therefore CN = 17 for $Gd_5Si_3B_{0.64}$ instead of CN = 15 for Gd_5Si_3 (Table 5). On the contrary, the CN remains equal to 14 for the Gd1 atoms in both structures, since they are not affected by additional B atoms. Finally, there is no metalloïd-metalloïd bond in both structures.

A more detailed analysis of the distances shows the slight decrease of the Gd2–Gd2 distances within the Gd_6 octahedra when boron is present. Indeed, the Gd2–Gd2 distances (Gd2–2Gd2 and Gd2–4Gd2) within the Gd_6 octahedron in $Gd_5Si_3B_{0.64}$ (3.552 and 3.807 Å, respectively) are smaller than the ones in Gd_5Si_3 (3.574 and 3.816 Å). The electronegativity of boron within the octahedron, in the ternary borosilicide, which attracts the electrons from the Gd2 atoms and constrains them to be more cationic, may explain the decrease of the Gd2–Gd2 distances and consequently the one of the unit cell parameters.

Attempts to obtain single crystals of sufficient size for electrical measurements are at the present time in

progress. In addition, the first theoretical calculations tend towards a metallic behavior for these compounds.

4. Conclusion

The isothermal section of the Gd–Si–B diagram has been proposed at 1270 K from bulk experiments by XRD, scanning electron microscopy and electron probe microanalysis. Prior to this work, the binary systems Gd–B, Gd–Si and Si–B have been re-investigated. Under our experimental conditions, the stable phases which border the diagram have been found to be Gd_5Si_3, Gd_5Si_4, GdSi, α-$GdSi_2$ and α-$GdSi_{2-x}$ in the Gd–Si system and Gd_2B_5, GdB_4 and GdB_6 in the Gd–B system. The binaries GdB_2 and GdB_{66} known in literature have not been obtained in the present study. For the more complex Si–B system, some inconsistencies with literature at the present time need that additional studies, especially on single crystals, must be done.

The main feature of the ternary diagram is the discovery of two gadolinium borosilicides $Gd_5Si_2B_8$ and $Gd_5Si_3B_{0.64}$. The X-ray structures of $Gd_5Si_3B_{0.64}$ and host binary Gd_5Si_3 have been determined on single crystals for comparison. They belong to the large family of compounds having the Mn_5Si_3-type. The only structural difference between both structures results from the partial occupancy by boron of the normally vacant interstitial site at the center of the Gd_6 octahedron, at the origin of the unit cell. It should be noted that the Gd_6 octahedra are stacked upon each other by common faces in order to generate infinite chains along the [001] direction. Strong bonding between the interstitial boron atoms and the gadolinium ones forming the Gd_6B polyhedra is indicated by the decrease in the corresponding Gd–Gd distances and consequently in the unit cell volume.

Acknowledgments

One of the authors (V.B) is grateful to the Centre National de la Recherche Scientifique (CNRS) for financial support through a research grant. The authors also thank T. Roisnel (Centre de Diffractométrie, Université de Rennes 1) for X-ray intensity data collection and fruitful discussions, J.C. Jegaden, O. Rastoix and J. Le Lannic (CMEBA, Université de Rennes 1) and M. Bohn (IFREMER, Brest) for their assistance in the SEM and EPMA studies.

References

[1] P. Rogl, H. Bittermann, Int. J. Refract. Metals Hard Mater. 17 (1999) 27–32.
[2] E. Bidaud, K. Hiebl, R.D. Hoffmann, R. Pöttgen, C. Jardin, J. Bauer, R. Gautier, P. Gougeon, J.Y. Saillard, J.F. Halet, J. Solid State Chem. 154 (2000) 286–295.
[3] O. Oeckler, C. Jardin, H. Mattausch, A. Simon, J.F. Halet, J.Y. Saillard, J. Bauer, Z. Anorg. Allg. Chem. 627 (2001) 1389–1394.
[4] O. Oeckler, J. Bauer, H. Mattausch, A. Simon, Z. Anorg. Allg. Chem. 627 (2001) 779–788.
[5] E. Bidaud, K. Hiebl, J. Bauer, J. Alloys Compd. 316 (2001) 75–81.
[6] F. Wittkar, J.F. Halet, J.Y. Saillard, P. Rogl, J. Bauer, Inorg. Chem. 33 (1994) 1297–1305.
[7] D. Ansel, J. Bauer, F. Bonhomme, G. Boucekkine, G. Frapper, P. Gougeon, J.F. Halet, J.Y. Saillard, B. Zouchoune, Angew. Chem. Int. Ed. Engl. 35 (1996) 2098–2101.
[8] J. Bauer, J.F. Halet, J.Y. Saillard, Coord. Chem. Rev. 178–180 (1998) 723–753.
[9] C. Jardin, O. Oeckler, H. Mattausch, A. Simon, J.F. Halet, J.Y. Saillard, Inorg. Chem. 39 (2000) 5895–5900.
[10] Yu.B. Kuz'ma, N.F. Chaban, Binary and Ternary Systems Containing Boron, Metallurgiya, Moscow, 1990.
[11] N.F. Chaban, Yu.B. Kuz'ma, Inorg. Mater. 36 (2000) 882–883.
[12] I. Mayer, I. Felner, J. Less-Common Met. 37 (1974) 171–173.
[13] I. Higashi, T. Tanaka, K. Kobayashi, Y. Ishizawa, M. Takami, J. Solid State Chem. 133 (1997) 11–15.
[14] F.X. Zhang, A. Sato, T. Tanaka, J. Solid State Chem. 164 (2002) 361–366.
[15] T. Mori, T. Tanaka, J. Solid State Chem. 154 (2000) 223–228.
[16] T. Tanaka, F.X. Zhang, A. Sato, Abstracts of the 14th International Symposium on Boron, Borides and related Compounds (ISBB'02), St. Petersburg, Russia, June 9–14, 2002, p. 44.
[17] T. Mori, T. Tanaka, Mater. Res. Bull. 36 (2001) 2463–2470.
[18] T. Tanaka, A. Sato, J. Solid State Chem. 165 (2002) 148–158.
[19] J.R. Salvador, D. Bilc, S.D. Mahanti, M.G. Kanatzidis, Angew. Chem. Int. Ed. 41 (2002) 844–846.
[20] F.D. Shepherd, A.C. Yang, IEDM Tech. Dig. (1973) 310–314.
[21] L. Pahun, Y. Campidelli, F. Arnaud d'Avitaya, P.A. Badoz, Appl. Phys. Lett. 60 (1992) 1166–1168.
[22] Y. Chen, D.A.A. Ohlberg, G. Medeiros-Ribeiro, Y.A. Chang, R.S. Williams, Appl. Phys. Lett. 76 (2000) 4004–4006.
[23] J.Y. Duboz, P.A. Badoz, F. Arnaud d'Avitaya, J.A. Chroozek, Appl. Phys. Lett. 55 (1989) 84–86.
[24] L.G. Aksel'rud, P.Yu. Zavalii, Yu.N. Grin, V.K. Pecharski, B. Baumgarter, E. Wölfel, Mater. Sci. Forum 335 (1993) 133–136.
[25] COLLECT: KappaCCD software, Nonius BV, Delft, The Netherlands, 1998.
[26] Z. Otwinowski, W. Minor, in: C.W. Carter Jr., R.M. Sweet (Eds.), Methods in Enzymology, Vol. 276, Academic Press, New York, 1997, pp. 307–326.
[27] A. Altomare, M.C. Burla, M. Camalli, G. Cascarano, C. Giacovazzo, A. Guagliardi, A.G.G. Moliterni, G. Polidori, R. Spagna, J. Appl. Crystallogr. 32 (1999) 115–119.
[28] K. Brandenburg, Diamond, Version 2.0, 1998.
[29] T.B. Massalski, Binary Alloy Phase Diagrams, 2nd Edition, ASM, Materials Park, OH, 1990.
[30] P. Villars, L.D. Calvert, Pearson's Handbook of Crystallographic Data for Intermetallic Phases, 2nd Edition, ASM, Materials Park, OH, 1991.
[31] R.F. Giese Jr., J. Economy, V.I. Matkovich, Z. Kristallogr. 122 (1965) 144–154.
[32] B. Armas, G. Male, D. Salanoubat, C. Chatillon, M. Allibert, J. Less-Common Met. 82 (1981) 245–254.
[33] Y. Imai, M. Mukaida, M. Ueda, A. Watanabe, J. Alloys Compd. 347 (2002) 244–251.
[34] M. Vlasse, G.A. Slack, M. Garbauskas, J.S. Kasper, J.C. Viala, J. Solid State Chem. 63 (1986) 31–45.
[35] M. Vlasse, J.C. Viala, J. Solid State Chem. 37 (1981) 181–188.

[36] L. Pauling, Nature of the Chemical Bond, 3rd Edition, Cornell Univ. Press, Ithaca, NY, 1960.
[37] V. Babizhetskyy, J. Roger, S. Députier, R. Guérin, J. Alloys Compd., to be submitted.
[38] T.L. Aselage, J. Mater. Res. 13 (1998) 1786–1794.
[39] V. Babizhetskyy, J. Roger, S. Députier, J. Bauer, R. Guérin, Abstracts of the 14th International Symposium on Boron, Borides and Related Compounds (ISBB'02), St. Petersburg, Russia, June 9–14, 2002, p. 64.
[40] R. Jardin, V. Babizhetskyy, R. Guérin, J. Bauer, J. Alloys Compd. 353 (2003) 233–239.
[41] A. Zalkin, D.H. Templeton, Acta Crystallogr. 6 (1953) 269–272.
[42] W.H. Zachariasen, Acta Crystallogr. 2 (1949) 94–99.
[43] V. Babizhetskyy, J. Roger, S. Députier, R. Jardin, J. Bauer, R. Guérin, K. Hiebl, C. Jardin, J.Y. Saillard, J.F. Halet, Angew. Chem. Int. Ed., to be submitted.
[44] B. Aronsson, Acta Chem. Scand. 14 (1960) 1414–1418.
[45] A.Z. Thom, V.G. Young, M. Akinc, J. Alloys Compd. 296 (2000) 59–66.
[46] H. Nowotny, in: P. Beck (Ed.), Electronic Structure and Alloy Chemistry of the Transition Elements, Wiley, New York, 1963, p. 179.
[47] F. Laves, Theory of Alloys Phases, ASM, Cleveland, OH, 1956.